Acta Crystallographica Section B
Structural Science
ISSN 0108-7681

Features of the electron density in magnesium diboride: reconstruction from X-ray diffraction data and comparison with TB-LMTO and FPLO calculations

V. Tsirelson,[a,b]* A. Stash,[c] M. Kohout,[a] H. Rosner,[a] H. Mori,[d] S. Sato,[e] S. Lee,[f] A. Yamamoto,[f] S. Tajima[f] and Yu. Grin[a]

[a]Max-Planck Institut für Chemische Physik fester Stoffe, Nöthnitzer Str. 40, Dresden 01187, Germany, [b]Quantum Chemistry Department, Mendeleev University of Chemical Technology, Moscow 125047, Russia, [c]Karpov Institute of Physical Chemistry, Moscow 103064, Russia, [d]Institute for Solid State Physics, University of Tokyo, 5-1-5 Kashiwanoha, Kashiwa, Chiba 277-8581, Japan, [e]Sato Laboratory, Kuboyama 1-9-109, Hachioji, Tokyo 192-0023, Japan, and [f]Superconductivity Research Laboratory, International Superconductivity Technology Centre, Shinonome, Koto-ku, Tokyo 135-0062, Japan

Correspondence e-mail: tsirel@muctr.edu.ru

Received 31 March 2003
Accepted 2 June 2003

Features of the electron density in MgB_2 reconstructed from room-temperature single-crystal X-ray diffraction intensities using a multipole model are considered. Topological analysis of the total electron density has been applied to characterize the atomic interactions in magnesium diboride. The shared-type B—B interaction in the B-atom layer reveals that both σ and π components of the bonding are strong. A closed-shell-type weak B—B π interaction along the c axis of the unit cell has also been found. The Mg—B closed-shell interaction exhibits a bond path that is significantly curved towards the vertical Mg-atom chain ([110] direction). The latter two facts reflect two sorts of bonding interactions along the [001] direction. Integration of the electron density over the zero-flux atomic basins reveals a charge transfer of $\sim$1.4 (1) electrons from the Mg atoms to the B-atom network. The calculated electric-field gradients at nuclear positions are in good agreement with experimental NMR values. The anharmonic displacement of the B atoms is also discussed. Calculations of the electron density by tight-binding linear muffin-tin orbital (TB-LMTO) and full-potential non-orthogonal local orbital (FPLO) methods confirm the results of the reconstruction from X-ray diffraction; for example, a charge transfer of 1.5 and 1.6 electrons, respectively, was found.

1. Introduction

Many papers dealing with the recently discovered superconductor MgB_2 (Nagamatsu *et al.*, 2001) discuss the chemical bonding in this compound. However, few papers deal with the electron density (ED) in MgB_2. The ED obtained by first-principle calculations in different schemes has been discussed by Belashchenko *et al.* (2001), Ravindran *et al.* (2001), Osorio-Guillen *et al.* (2002) and Mazin & Antropov (2003). Three other papers deal with ED derived from X-ray diffraction experiments; Lee *et al.* (2001) and Mori *et al.* (2002) have presented Fourier maps of the total and deformation EDs using room-temperature single-crystal measurements, while Nishibori *et al.* (2001) have mapped the total ED reconstructed by the maximum-entropy method from synchrotron radiation powder data at 295 and 15 K. An attempt to perform a single-crystal study by electron diffraction has also been undertaken (Jiang *et al.*, 2002). Both theoretical and experimental work has considered only a very general picture of the electron distribution in magnesium diboride.

In this paper, we report a detailed study of the electron-density features in MgB_2, reconstructed from accurate room-temperature single-crystal X-ray diffraction intensities using a multipole model. We analyze the ED in term of Bader's topological theory, which uses the gradient field and the

Laplacian of the ED to characterize the atomic interactions in a crystal (Bader, 1990). The results from reconstruction of the experimental ED are compared with those calculated using tight-binding linear muffin-tin orbital (TB-LMTO) and full-potential non-orthogonal local orbital (FPLO) methods. We also discuss the anharmonic atomic displacements of the B atoms in MgB_2.

2. Treatment of the experimental data

Preparation of the single crystals of MgB_2 as well as the details of the room-temperature X-ray (Mo $K\alpha$) data collection are described in detail by Mori *et al.* (2002). The 889 measured reflections ($-8 \le h \le 8$, $-8 \le k \le 8$ and $-9 \le l \le 9$) were corrected for Lorentz and polarization effects. Absorption was taken into account numerically according to the procedure of Akselrud *et al.* (1990) ($T_{\min} = 0.9445$, $T_{\max} = 0.9502$ and $R_{\rm eq} = 0.0216$). The 108 averaged symmetry-independent non-zero reflections [$I > 3\sigma(I)$] have been used in the following analysis.

The model used for the treatment of the X-ray diffraction data was as follows. The ED was approximated by the Hansen & Coppens (1978) multipole model as a superposition of the atomic electron densities in the form

$$\rho_{\rm atomic}(\mathbf{r}) = \rho_{\rm core}(r) + P_v \kappa'^3 \rho_{\rm spher,valence}(\kappa' r) + \sum_{l=1}^{4} \kappa''^3 R_l(\kappa'' r) \sum_{m=-l}^{l} P_{lm\pm} y_{lm\pm}(\mathbf{r}/r).$$

In this expression, the ED of the atomic cores, $\rho_{\rm core}$, is considered to be undisturbed by chemical bonds, while $\rho_{\rm spher,valence}$ describes the spherical deformation of the atomic valence shell in a crystal; both densities were calculated from atomic wavefunctions. The valence ED of each atom was additionally expanded in a Laplace series over the real spherical harmonics $y_{lm\pm}$ satisfying the symmetry of the local atomic environment. Slater-type radial functions, $R_l \simeq r^{n_l} \exp(-\kappa'' \xi r)$, were used to describe the r dependence of atomic multipoles. The atomic valence-shell contraction/expansion κ' and κ'' parameters and the electron populations P_v and $P_{lm\pm}$ were determined by the least-squares adjustment of the model structure amplitudes to fit the experimental ones.

The symmetry of the Mg-atom position is 6/*mmm*, while boron is sited in a $\overline{6}m2$ position (space group $P6/mmm$). Therefore, at the hexadecapole level of the multipole model ($l_{\max} = 4$), only P_v, P_{20} and P_{40} for Mg atoms and P_v, P_{20}, P_{33-} and P_{40} for B atoms will be allowed by the symmetry. The core and valence EDs were described by the atomic many-configuration relativistic wavefunctions of Macchi & Coppens (2001). The respective radial-function parameters $n_2 = n_4 = 4$ and $\xi_{\rm Mg} = 3.4$ for Mg, and $n_2 = 2$, $n_3 = 3$, $n_4 = 4$ and $\xi_{\rm B} = 3.0$ for B, have been used. Anomalous dispersion corrections were taken from the *International Tables for Crystallography* (1995, Vol. C), and an isotropic secondary extinction correction according to Becker & Coppens (1974) was applied.

The anharmonicity of the atomic displacements was modeled using the Gram–Charlier expansion of temperature factors up to the tensors of fourth rank (*International Tables for Crystallography*, 1995, Vol. C)

$$T_\mu(\mathbf{h}) = T_\mu^{\rm harm}(\mathbf{h})\{1 + [(2\pi i)^3/3!]C^{pqr} h_p h_q h_r + [(2\pi i)^4/4!]D^{pqrs} h_p h_q h_r h_s\}.$$

$T_\mu^{\rm harm}(\mathbf{h})$ takes into account the harmonic displacements of atom μ from its equilibrium position, C^{pqr} and D^{pqrs} are the third- and fourth-order anharmonic displacement parameters, respectively, and $\mathbf{h}$ is the scattering vector with components $h_i = h, k, l$ ($i = p, q, r$ and s). Owing to symmetry restrictions, only the following (symmetry-independent) anharmonic displacement parameters in MgB_2 differ from zero: D^{1111}, D^{3333} and D^{1133} for Mg atoms, and C^{111}, D^{1111}, D^{3333} and D^{1133} for B atoms.

Refinement of the structural model was carried out with the *MOLDOS*02 program (Stash, 2002) based on the program *MOLLY* (Hansen & Coppens, 1978; Protas, 1997). Initially, we carried out a conventional spherical-atom harmonic refinement and confirmed the small Mg-position depopulation that results in the composition $Mg_{0.955(5)}B_2$, as derived by Mori *et al.* (2002) for the same crystal. This result also agrees with the X-ray powder data analysis of Schmidt *et al.* (2003). In addition, we checked and excluded the possibility of Mg disorder along the *c* axis (in good agreement with the recent results for aluminium diboride; Burkhardt *et al.*, 2003). Subsequently, we fixed the occupancy of the Mg-atom position and applied a more complicated multipole model, as well as taking into account the anharmonicity of atomic displacement. Preliminary analysis has shown that the anharmonic displacement parameters of the Mg atom are small and do not exceed 2 s.u., and a strong correlation between the displacement parameters and the multipole parameters was observed for Mg. We have also found the hexadecapole multipole parameters of both Mg and B atoms to be statistically insignificant. Therefore, only the multipole parameters P_v and P_{20} for Mg atoms, and P_v, P_{20} and P_{33-} for B atoms were included in the final model. Mg atoms were considered in a harmonic approximation, while B atoms were described in an anharmonic approximation.

The refinement procedure, which allowed approximate separation of the ED features and the atomic displacement anharmonicity, was as follows. In accordance with the method of Sasaki *et al.* (1980), the valence electron population of Mg was changed with a step size of 0.1 e in the range $0.6\ {\rm e} \le P_v \le 1.2\ {\rm e}$; the electroneutrality condition was retained for the unit cell. Then, starting from the atomic harmonic displacement parameters of Mori *et al.* (2002), all the displacement parameters were refined using reflections with $\sin\theta/\lambda \ge 0.6\ {\rm \AA}^{-1}$, while the scale factor and the κ' and $P_{lm\pm}$ parameters were refined with all reflections. Such a procedure was repeated several times for each value of the valence electron population of atoms. The weighting scheme $w = \sigma^2_{\rm statistics}(F) + (0.01F)^2$ was used. The optimal $P_{\rm v}$ value was chosen by interpolation according to the lowest R_w value, as suggested by Voloshina *et al.* (1989), and was fixed. The extinction parameter was included in the refinement in the same iterative manner as described above. The refinement

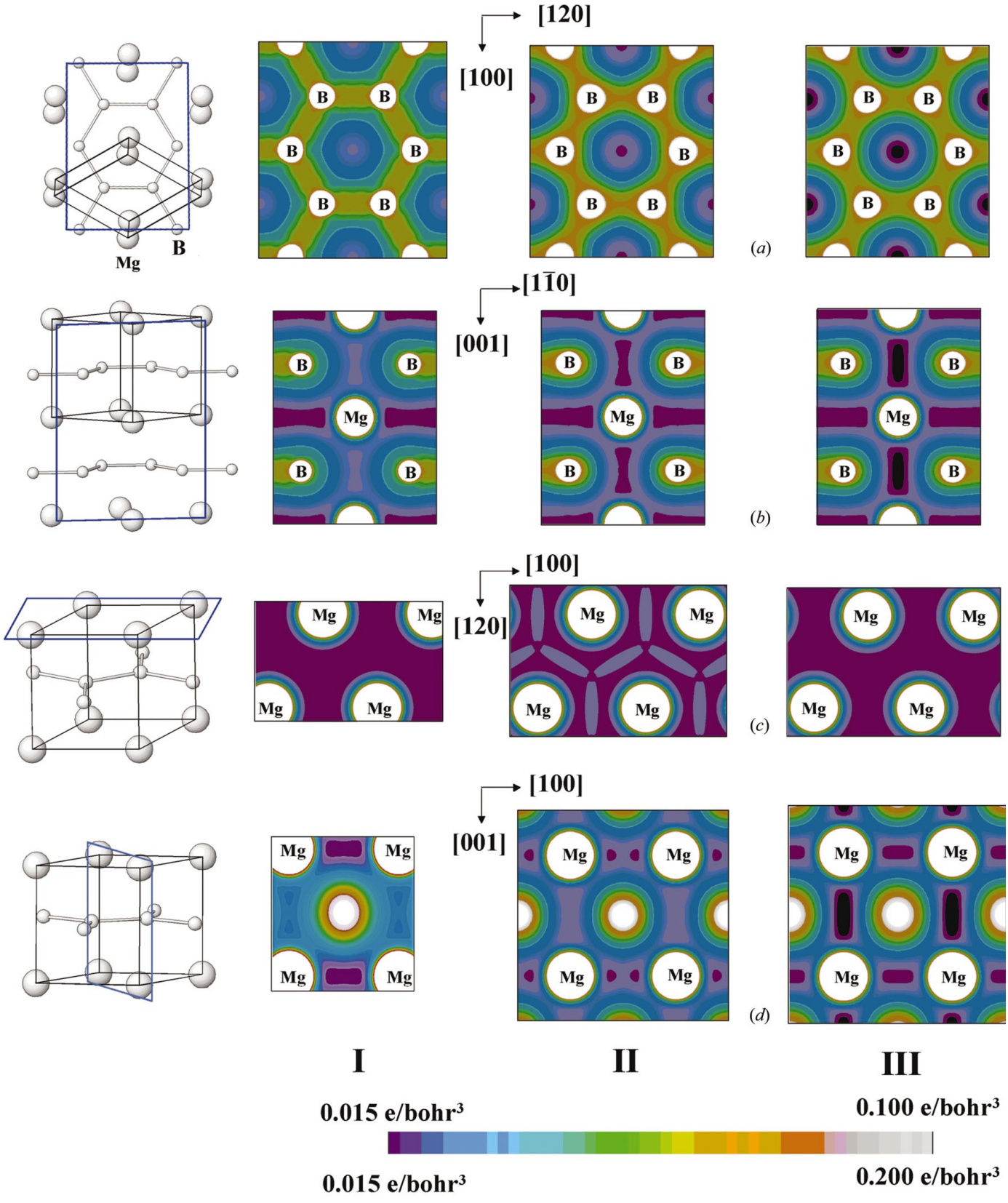

Figure 1
Electron-density maps in structurally relevant planes in MgB_2: (I) reconstructed from the X-ray diffraction data, (II) calculated by the TB-LMTO method and (III) calculated by the FPLO method. (*a*) The B-atom network plane. (*b*) Plane (1$\bar{1}$0), perpendicular to the B-atom network plane. (*c*) Mg-atom plane. (*d*) Plane (100), perpendicular to the B—B bond. The upper scale is valid for (*a*) and (*b*), and the lower scale is valid for (*c*) and (*d*). The unit cell and the map planes are also shown.

Table 1
Atomic coordinates and multipole parameters of MgB_2 [space group $P6/mmm$, a = 3.0846 (8) Å and c = 3.5199 (8) Å].

Reliability factors are $R(F) = 0.009$, $R_w(F) = 0.012$, $R(F^2) = 0.015$, $R_w(F^2) = 0.023$ and $S = 100$.

Atomic coordinates and multipole parameters	Mg (in 6/*mmm*)	B (in $\bar{6}m2$)
x	0	1/3
y	0	2/3
z	0	1/2
SOF	0.955 (5)	1
κ'	1.01 (12)	0.89 (1)
ξ	3.4	3.0
P_v	0.825 (50)†	3.562 (50)†
P_{20}	0.063 (34)	−0.058 (16)
P_{33-}	–	−0.139 (23)

† P_v values were determined by interpolation of the step-wise refinement results (see text for details). The standard deviation of these values was taken as half of the step.

Table 2
Harmonic and anharmonic atomic displacement parameters (ADPs) for MgB_2.

ADP	Mg	B
U^{11} (Å^2)	0.00516 (3)	0.0065 (2)
U^{22} (Å^2)	U^{11}	U^{11}
U^{33} (Å^2)	0.00578 (5)	0.0079 (3)
U^{12} (Å^2)	$0.5U^{11}$	$0.5U^{11}$
C^{111} (10^3 Å^3)	–	−0.00007 (220)
D^{1111} (10^4 Å^4)	–	0.00627 (173)
D^{3333} (10^4 Å^4)	–	0.00640 (178)
D^{1133} (10^4 Å^4)	–	0.01227 (360)

converged well; the maximal correlation (correlation coefficient 0.94) was observed between the U^{11} and D_{3333} displacement parameters of the B atom. The lowest extinction factor, $y_{\min} = 0.93$, was found for the 200 reflection ($I_{obs} = y I_{kin}$, where I_{obs} and I_{kin} are the observed and kinematic intensities, respectively).

The final reliability factors, multipole parameters and other model parameters are given in Table 1, and the atomic displacement parameters are listed in Table 2.

The multipole parameters obtained were used to calculate both the total and the deformation ED maps of the static model (the latter characterizes the redistribution of electrons in relation to a crystal built from spherical atoms). The total ED maps in the relevant planes in the MgB_2 structure are shown in Fig. 1. A topological analysis of the total model ED (Bader, 1990) was also performed; maps of the gradient field of the ED (Fig. 2) and the Laplacian of the ED (Fig. 3) were calculated, and features of the critical points in the ED were estimated (Table 3). Deformation ED maps in the selected planes were also calculated (Fig. 4). All calculations were performed with the *WinXPRO* program (Stash & Tsirelson, 2002).

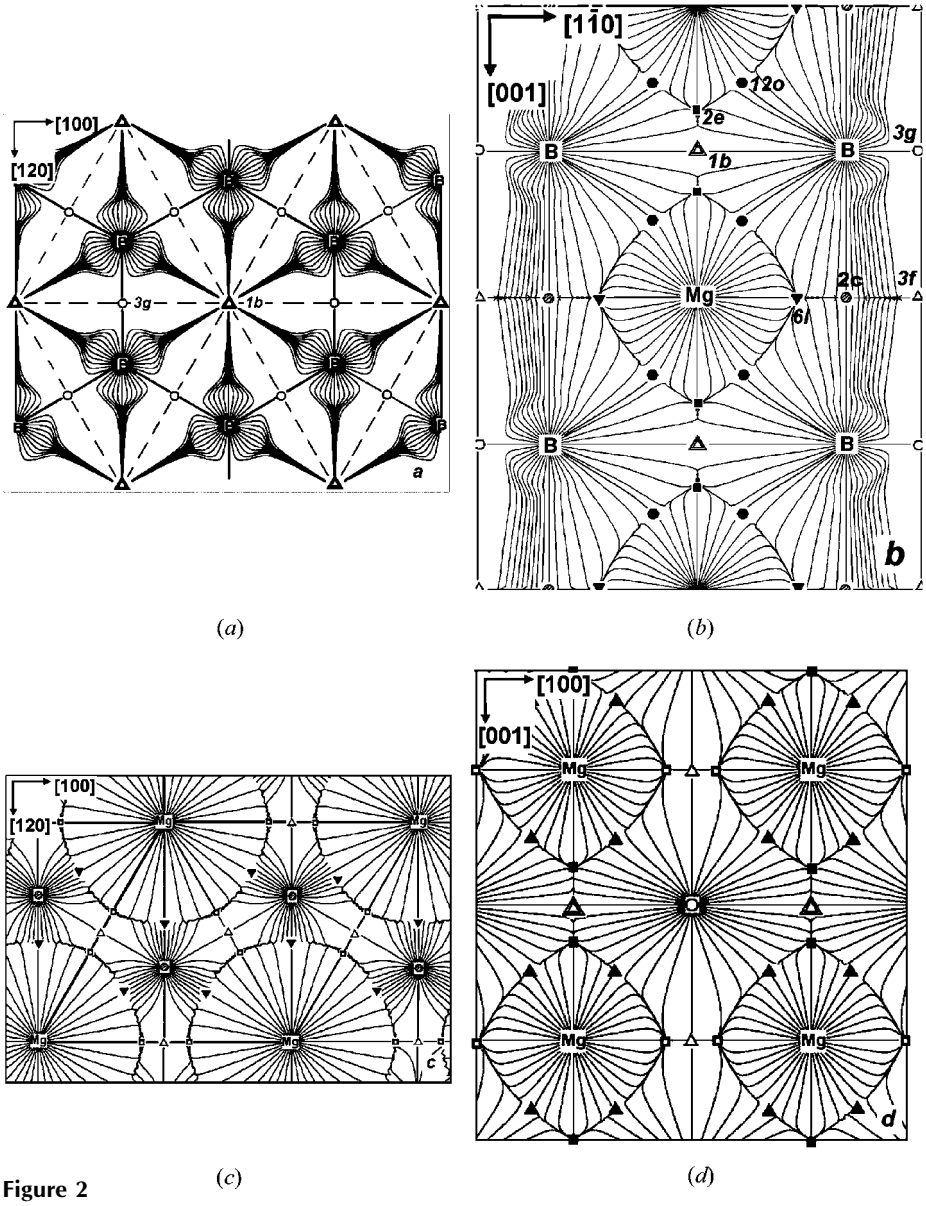

Figure 2
Gradient field of the electron density in structurally relevant planes in MgB_2. (*a*), (*b*), (*c*) and (*d*) are as described in the caption to Fig. 1. Critical points are given according to Table 3.

3. Theoretical calculations

In order to obtain an independent estimate of the accuracy of the ED reconstructed from experimental data, we performed electronic structure calculations using two different methods based on the local-density approximation, namely the TB-LMTO (tight-binding linear muffin-

Table 3
Topological characteristics of the critical points (CPs) for MgB_2 determined from the reconstructed experimental ED (*cf.* Fig. 2).

Wyckoff notation and position of CP	$\rho(\mathbf{r}_{CP})$ (e Å^{-3})	$\nabla^2\rho(\mathbf{r}_{CP})$ (e Å^{-5})	λ_1 (e Å^{-5})	λ_2 (e Å^{-5})	λ_3 (e Å^{-5})	Type of CP
1(*b*) (0, 0, 0.5)	0.171 (15)	0.77 (20)	−0.05	0.41	0.41	(3,+1)
2(*c*) (1/3, 2/3, 0)	0.109 (12)	0.41 (18)	−0.04	−0.04	0.49	(3,−1)
2(*e*) (0, 0, 0.374)	0.168 (14)	0.72 (20)	0.14	0.29	0.29	(3,+3)
3(*f*)(0.5, 0, 0)	0.104 (12)	0.39 (8)	−0.04	0.03	0.40	(3,+1)
3(*g*) (0.5, 0, 0.5)	0.810 (16)	−4.63 (30)	−3.52	−2.70	1.59	(3,−1)
6(*j*) (0.408, 0, 0)	0.103 (12)	0.51 (19)	0.02	0.11	0.37	(3,+3)
6(*l*) (0.229, 0.458, 0)	0.105 (12)	0.57 (19)	−0.02	0.20	0.39	(3,+1)
12(*n*) (0.184, 0, 0.254)	0.190 (11)	1.47 (22)	−0.28	0.01	1.74	(3,+1)
12(*o*) (0.106, 0.212, 0.253)	0.191 (11)	1.47 (22)	−0.27	−0.01	1.75	(3,−1)

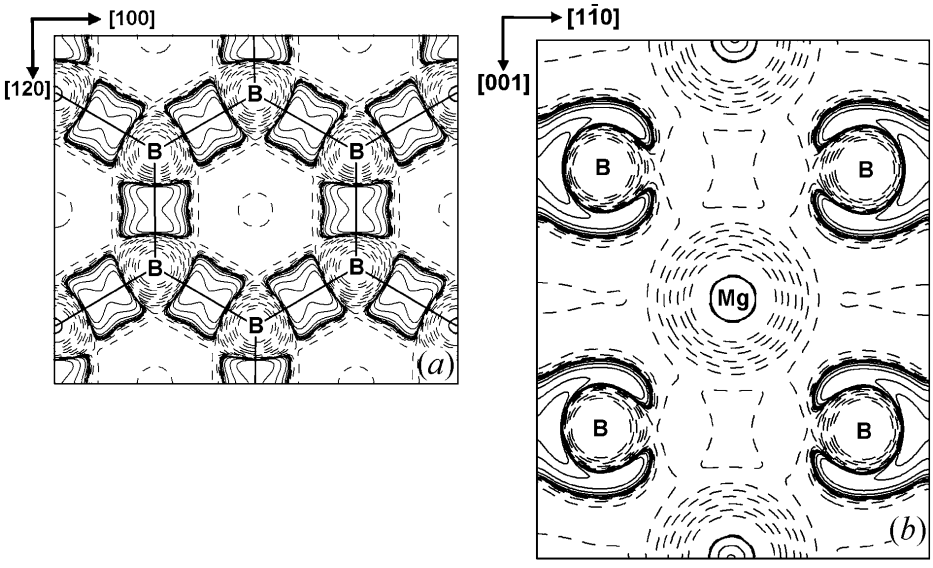

Figure 3
Laplacian of electron-density maps for MgB_2. Sections in (*a*) the B-atom network plane and (*b*) the (1$\bar{1}$0) plane are shown. Solid and broken lines represent negative and positive Laplacian values, respectively. Line intervals are $\pm2 \times 10^n$, $\pm4 \times 10^n$ and $\pm8 \times 10^n$ e Å^{-5} ($-2 \leq n \leq 2$).

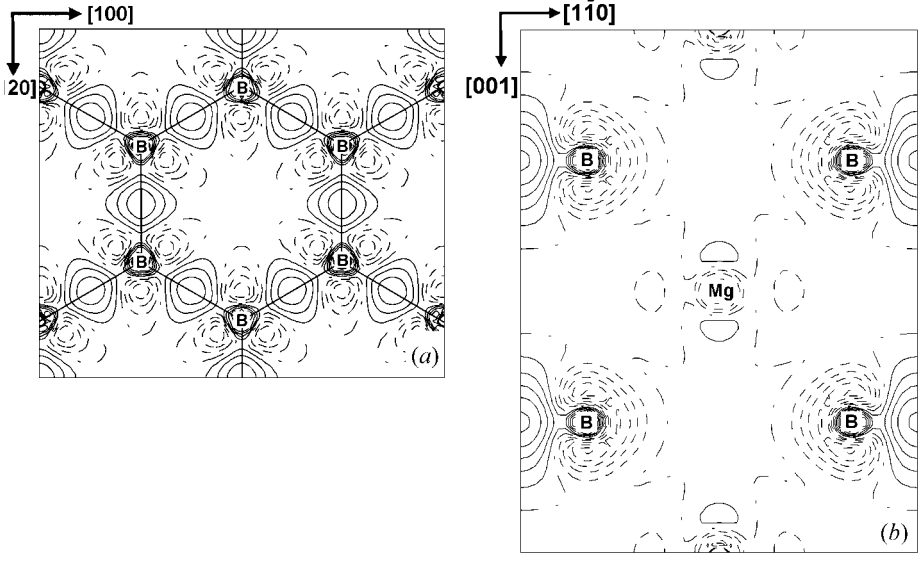

Figure 4
Deformation electron-density maps for MgB_2. Sections in (*a*) the B-atom network plane and (*b*) the (1$\bar{1}$0) plane are shown. Solid and broken lines represent excessive and deficient density values, respectively. The line interval is 0.05 e Å^{-3}.

tin orbital) and FPLO (full-potential non-orthogonal local orbital) methods.

For the TB-LMTO calculations, the *TB-LMTO-ASA* program package (Jepsen & Andersen, 1999), with exchange correlation potential according to Barth & Hedin (1972), was used. The radial scalar-relativistic Dirac equation was solved to obtain the partial waves. The calculation within the atomic sphere approximation (ASA) includes corrections for the neglect of interstitial regions and partial waves of higher order (Andersen *et al.*, 1986). In the case of MgB_2, the addition of empty spheres was not necessary. The following atomic-sphere radii were applied for the calculations: r(Mg) = 1.648 Å and r(B) = 0.970 Å.

The FPLO calculations used the Koepernik & Eschrig (1999) code, and the Perdew & Wang (1992) parameterization was applied for the exchange and correlation potentials. Mg (3*s*3*p*3*d*) and B (2*s*2*p*3*d*) states were chosen as the basis set, and all lower-lying states were treated as core states. The 3*d* states were taken into account in order to obtain a more complete basis set. The spatial extension of the basis orbitals, controlled by a confining potential $(r/r_0)^4$ (Eschrig, 1989), was optimized to minimize the total energy. Brillouin zone integrations were performed using the tetrahedron method. Convergence with respect to the basis set and the *k*-mesh was carefully checked. For more details see Rosner *et al.* (2002).

The results of both calculation schemes are very similar. Comparing

standard features like the density of states and the band structure, we found a good overall agreement for the occupied states, with a bandwidth of 12 eV in both calculations. Small deviations appear on an energy scale of 200 meV, and these are caused by a shift of the B $2p$-σ derived states *versus* the B $2p$-π derived states. Real-space charge densities should be affected even less by this shift, because it takes place in the energy reciprocal space.

Theoretical ED maps are given in Fig. 1, which allows a comparison with the reconstructed ED from the experimental data. Topological analysis of the calculated electron densities was performed with the program package *BASIN* (Kohout, 2002). Atomic ED basins estimated from calculations and from the reconstructed ED are presented in Fig. 5.

4. Discussion

X-ray elastic diffraction at some fixed temperature provides averaged atomic displacements (Table 2), which cannot be separated into dynamic and static contributions and which do not allow analysis of the vibration modes.[1] Thus, we cannot directly compare the results of Table 2 with the mode analysis performed by theoretical, spectroscopic or inelastic scattering methods (Goncharov *et al.*, 2001; Kunc *et al.*, 2001; Yildirim *et al.*, 2001). The use of a multipole model instead of simple spherical atoms did not change the atomic displacement parameters of the Mg atom (Mori *et al.*, 2002), while the harmonic displacement parameters of B increased by 20–30%. After anharmonicity was taken into account, the harmonic room-temperature amplitude of the B-atom displacement along the [001] direction became about 10% larger than the displacement in the (001) plane. The quartic anharmonicity has led to additional B-atom displacement along the B—Mg line.

Conventional X-ray experiments yield the dynamic ED averaged over the thermal motion (Tsirelson & Ozerov, 1996). The multipole model allows the derivation of the electron density, which is approximately deconvoluted from the thermal motion and extrapolated to a resolution of *ca* 0.1 Å. The first question that must be answered is how physically significant are the ED features derived from a complicated structural model such as that described above. Fortunately, we have an opportunity to gather some evidence in favor of the derived multipole ED of MgB_2. Indeed, the electron distribution (together with the nuclear-charge contribution) directly determines the electric-field gradient (EFG) at nuclear positions and, therefore, defines the quadrupole interaction constant, which is measured in the NMR experiment. The crystal structure of MgB_2 consists of alternating boron honeycomb sheets and hexagonal layers of Mg atoms. Owing to the symmetry, the EFGs, ∇E_{ii}, at the B and Mg nuclei are determined by only one independent component. The multipole model allows us to obtain a simple approximation of the electronic contribution to the EFG in the form (Tsirelson & Ozerov, 1996)

$$\nabla E^0_{zz} = 0.842\xi^3 P_{20}$$

(in units of 10^{21} V m^{-2}). P_{20} is the electron population of the quadrupole density term of the corresponding pseudo-atom, and ξ is the radial exponent in the quadrupole-term radial function (Table 1). The above expression yields $\nabla E^0_{zz} = -1.31\ (35) \times 10^{21}$ V m^{-2} for the B atom. Taking into account the lattice EFG contribution, $\nabla E^{\rm lat}_{zz} = 0.06 \times 10^{21}$ V m^{-2} (Medvedeva *et al.*, 2001), we arrive at the value $\nabla E_{zz} = -1.25\ (35) \times 10^{21}$ V m^{-2}, which agrees with the EFG absolute value deduced from the ^{11}B NMR experiment ($|\nabla E^{\rm exp}_{zz}| = 1.69 \times 10^{21}$ V m^{-2}; Gerashenko *et al.*, 2002) and the theoretically calculated value ($\nabla E^{\rm theor}_{zz} = -1.88 \times 10^{21}$ V m^{-2}; Medvedeva *et al.*, 2001). A similar calculation for the Mg atom yields $\nabla E_{zz} = 0.21\ (11) \times 10^{21}$ V m^{-2}, which agrees with the value from LAPW calculations ($\nabla E^{\rm theor}_{zz} = 0.27 \times 10^{21}$ V m^{-2};

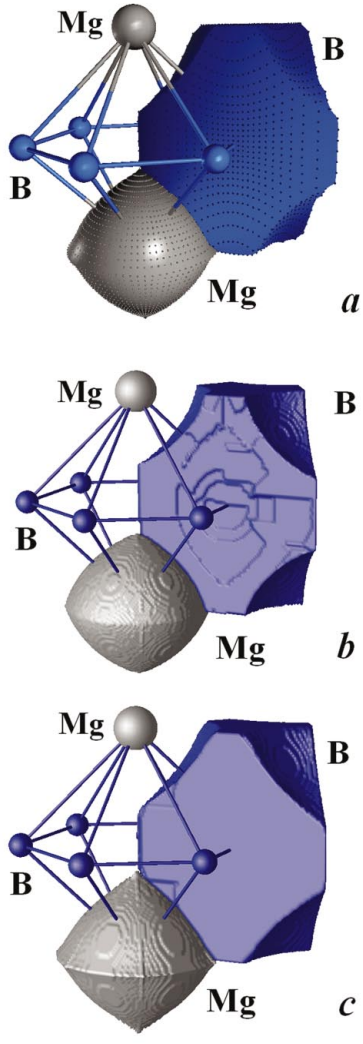

Figure 5
Zero-flux atomic basins in the electron-density distribution in MgB_2 (*a*) determined from X-ray structure factors, (*b*) calculated by the TB-LMTO method and (c) calculated by the FPLO method.

[1] Atomic positions in MgB_2 are fixed by symmetry; therefore, static displacements in this crystal may result from the small depopulation of the Mg-atom position.

Haas, 2001). Thus, the quasi-static multipole ED reconstructed from the X-ray diffraction data is accurate enough to act as a bridge between the X-ray diffraction and NMR experiments, and therefore it is worth considering the ED features in more detail.

Topological features of the ED – *i.e.* the gradient vector field $\nabla\rho(r)$, the positions and characteristics of the critical points [CP; the points where $\nabla\rho(r_c) = 0$], and the Laplacian of the ED – reflect the driving forces responsible for bonding in molecules and crystals (Bader, 1990). Critical points are distinguished according to their rank and signature, where the rank is the number of non-zero eigenvalues, λ_i, of the ED curvature (Hessian) matrix and the signature is the sum of the algebraic signs of λ_i. The ED has four kinds of non-degenerate CPs of rank 3, *viz.* maxima (3,−3), minima (3,+3) and two types of saddle points, (3,+1) and (3,−1), which correspond to the nuclear positions, cages, rings and bonds in a molecule or crystal.

Consideration of the ED gradient field reveals that some atoms are connected by the lines that are formed by the gradient line pairs originating at a (3,−1) CP and terminating at two neighboring nuclei; the ED is maximal along these lines with respect to any neighboring line (*cf.* CP 3*g* in Figs. 2*a* and 2*b*, CP 2*c* in Fig. 2c, and CP 12*o* in Fig. 2*b*). These lines are called bond paths, and hence the associated (3,−1) critical points are termed the bond CPs. The parameters $\lambda_1 < 0$ and $\lambda_2 < 0$ measure the degree of ED contraction towards the (3,−1) CP along the directions normal to the bond path; $\lambda_3 > 0$ measures the degree of ED shift towards each of the connected nuclei. The existence of the (3,−1) CP (or the bond path) between two atoms is a necessary condition for the chemical bond to exist between these atoms (Bader, 1990).

The Laplacian of the ED, $\nabla^2\rho(\mathbf{r})$, characterizes the concentration and depletion of electrons at each point, $\mathbf{r}$, in a crystal (Bader, 1990). The sign of $\nabla^2\rho(\mathbf{r}_b) = \lambda_1 + \lambda_2 + \lambda_3$ at the (3,−1) CP depends on the relation between the principal curvatures of the ED and therefore reflects the character of the atomic interactions. If the electrons are locally concentrated around the bond CP position, $\mathbf{r}_b$ [$\nabla^2\rho(\mathbf{r}_b) < 0$], then electrons are shared by both nuclei [shared atomic interactions, *cf.* Figs. 3*a* and 3*b* for CP 3(*g*)]; this situation is typical for covalent bonding. The case where $\nabla^2\rho(\mathbf{r}_b) > 0$ corresponds to closed-shell interactions [*cf.* Table 3 for CP 2(*c*) and 12(*o*)].

The maps of the Laplacian of the ED show that electrons are concentrated both on the B—B lines and in areas spanning the B-atom positions in the plane perpendicular to the B—B bond (Fig. 3). The latter fact might be treated as a sign of π-like electron delocalization over the B-atom network. Mg atoms form a three-dimensional network of positive Laplacian regions with electron depletion. This network brings to light the structure of the electron-donor fragments of the MgB_2 structure.

The bond critical points on the B—B lines along the *c* axis of the unit cell [2(*c*) position] and the Mg—B lines [12(*o*) position] both indicate corresponding closed-shell-type interactions. The (3,−1) CP at 2(*c*) (Fig. 2) could hardly be predicted *a priori*; in a MgB_2 procrystal, the (3,+3) CP is observed at this point. According to Bader (1990), we can suppose that the appearance of this (3,−1) CP may reflect some additional bonding interaction between the boron layers in MgB_2. The possibility of such an interlayer interaction has been mentioned by Osorio-Guillen *et al.* (2002).

All of the CP types are present in the ED of MgB_2 (Table 3); the numbers of the different CP types obey the Poincare–Hopf–Morse condition (Zou & Bader, 1993; Martin Pendas *et al.*, 1997) and their positions are restricted by the space-group symmetry. No non-nuclear attractors were found. To check the physical significance of the topological ED features, the electronic potential density, $v(\mathbf{r})$, was calculated from the ED by a combination of the local virial theorem and the density-functional approximation for the kinetic energy density (Espinosa *et al.*, 1998; Tsirelson, 2002).[2] It is found that $v(\mathbf{r})$ is negative everywhere and all bond paths in the ED are homeomorphically mirrored in $-v(\mathbf{r})$, in agreement with a general consideration (Keith *et al.*, 1996). The (3,−1) CP in the model ED on the B—B lines in the boron layer [3(*g*) position] indicates a shared-type B—B interaction with significant bond ellipticity ($\varepsilon = \lambda_1/\lambda_2 - 1 = 0.3$) dominating perpendicular to the boron layers. Such a situation is typical for covalent bonds with a strong π component (Bader, 1990). Deformation ED maps (Fig. 4) explicitly confirm this feature. We note also the influence of Mg atoms situated in the (100) plane around the middle point of the B—B line [Figs. 1*d* (I) and 2*d*] favoring ED polarization along the [001] direction.

A conclusion about the presence of an Mg—B bond path is uncertain; the numerical difference between the characteristics of the (3,−1) CP at the 12(*o*) position and the (3,+1) CP at the 12(*n*) position (Table 3) is smaller than the experimental error. However, we should stress that both kinds of critical points are reproduced in both the electron density and the negative potential electron density. At the same time, the (3,−1) CP at the 12(*o*) position and the (3,+1) CP at the 12(*n*) position are close to being degenerate; one of the principal curvatures of the ED, λ_2, is always close to zero (Table 3). According to Bader (1990), degenerate critical points are unstable and the presence of such CPs in the electron-density distribution indicates that MgB_2 is close to structural instability. This observation is in line with the conclusion of Mazin & Antropov (2003) that the whole set of MgB_2 properties demonstrates that this compound probably exists at the brink of structural stability. Under these circumstances, the quartic anharmonicity of the B-atom displacement mentioned above may reflect either the dynamic Mg—B interaction or

[2] Potential energy density, $v(\mathbf{r}) < 0$, can be approximated using the local form of the virial theorem (Bader & Beddall, 1972),

$$2g(\mathbf{r}) + v(\mathbf{r}) = (\hbar^2/4m)\nabla^2\rho(\mathbf{r}),$$

and the gradient $\hbar$ expansion of the Green function around the classical Thomas–Fermi approximation (Kirzhnits, 1957), which yield the expression for kinetic energy density,

$$g(\mathbf{r}) = (3\hbar^2/10m)(3\pi^2)^{2/3}\rho(\mathbf{r})^{5/3} + (\hbar^2/72m)[\nabla\rho(\mathbf{r})]^2/\rho(\mathbf{r}) + (\hbar^2/6m)\nabla^2\rho(\mathbf{r}),$$

where $\hbar$ is the Planck constant and m is electron mass.

the static displacement of the B atoms in the vicinity of magnesium defects.

It is worth noting some additional observations concerning the Mg—B interaction. First, the Mg—B bond path is significantly curved; the shift of the CP from the Mg—B straight line towards the vertical Mg chain ([110] axis) is 0.21 Å. Second, the ratio $g(\mathbf{r})/\rho(\mathbf{r}) = 0.53$ is close to that expected in the case of shared interactions, while the ratio $\lambda_1/\lambda_3 = 0.15$ fits closed-shell (ionic) interactions (Bader, 1990). All these facts can be considered as an indication of the multicenter nature of the Mg—B interaction.

In the ED distribution, the areas around nuclear positions are separated by the unique surfaces where the ED gradient vector flux through these surfaces is zero

$$\nabla_i \rho(\mathbf{r}_i) \cdot \mathbf{n}_i(\mathbf{r}_i) = 0, \quad \forall \mathbf{r}_i \in S_i,$$

where $\mathbf{n}_i(\mathbf{r}_i)$ is a unit vector normal to the surface S_i at point $\mathbf{r}_i$. Thus, a zero-flux surface S_i defines the basin of each atom (Bader, 1990). Atomic zero-flux shapes of the atoms in MgB_2 are depicted in Fig. 5. It can be seen that Mg is well described by a sphere of radius $r = 1.06$ Å [neglecting small spikes that were found for other cations by Luana *et al.* (1997)]. At the same time, the zero-flux surface of the B atom has a complicated shape.

Integration of the model ED over the atomic basins allows the atomic electron populations to be estimated. Such integration results in electron counts of $Q(Mg_{0.955}) = 10.05$ (4) e and $Q(B) = 5.66$ (3) e if deficiency of the Mg position is taken into account. The total number of electrons in the $Mg_{0.955}B_2$ unit cell is 21.46, while integration yields 21.37. Thus, a charge transfer of *ca* 1.4 (1) e from a basin volume assigned to magnesium [5.37 (1) Å^3] to the B-atom network [with a volume of 11.84 (1) Å^3 per atom] takes place.

The calculated ED [Figs. 1(II) and 1(III) for FPLO and LMTO results, respectively] is topologically very similar to that reconstructed from the experimental data. Especially remarkable is the landscape in the [100] section through the Mg-atom positions. The double-minima distribution with a saddle (3,+1) critical point between Mg atoms is observed in both the calculated and the reconstructed ED (Fig. 1*d*). This pattern is also valid for the region of the boron–boron covalent interaction (Fig. 1*b*), although calculations did not show the ellipticity of the B—B bond mentioned above.

The two different methods of calculation yield very similar results. The atomic basins evaluated from both TB-LMTO and FPLO calculations have nearly identical shapes (Fig. 5). A small difference between the LMTO and FPLO densities appears in the spike-like features for the magnesium basin, which are more pronounced in the full-potential calculation and correlate remarkably well with the results from the model-reconstructed ED. Because the density in this region is low and the region itself is relatively small, these differences have a negligible influence on integrated properties like the charge for Bader's atoms.

The integration of the ED in the atomic basins (for both methods of calculation) gives the transfer of 1.5 (TB-LMTO) or 1.6 (FPLO) electrons from the Mg atoms to the B-atom network. The correlation of this value with the reconstructed ED results (1.4 e) is remarkable, and these values are also close to the charge transfer calculated from the P_v parameters of the multipole model (Table 1).

Note also that the charge transfer of 1.5 (TB-LMTO), 1.6 (FPLO) or 1.4 electrons (from reconstructed density) from the magnesium to boron network correlates well with the results of bonding analysis in magnesium diboride with the electron localization function (Schmidt *et al.*, 2003). The latter revealed a charge of 2.5 e for each B—B bond: it corresponds to a charge transfer of 1.5.

The above-mentioned good agreement between experimental and theoretical ED demonstrates that the measured intensities were not significantly affected by diffuse scattering resulting from defects of the crystal sample used in the X-ray diffraction experiment [for experimental observations from the powder data see Zhu *et al.* (2001)].

The good agreement of the reconstructed ED for a real crystal with the electronic structure calculations for the idealized lattice indirectly supports the theoretical conclusions concerning the superconducting properties of MgB_2. Band-structure calculations by Kortus *et al.* (2001), An & Pickett (2001) and Belashchenko *et al.* (2001) indicated that MgB_2 possesses essentially metallic boron states, with both p_σ and p_π bands at the Fermi level. The ionization of Mg atoms promotes the generation of holes in the valence band (An & Pickett, 2001). The charge transfer implied by our experimental and theoretical results corresponds to partially ionic Mg—B bonding, in contrast to the fully ionic bonding that is often assumed in the literature. Although a direct connection between the real-space ED and the superconductivity cannot be drawn, the indirect link *via* electronic structure calculations underlines the reliability of the present theories about superconductivity in MgB_2.

In conclusion, the features of the atomic interactions in MgB_2 have been elucidated using the reconstructed experimental (X-ray) ED and theoretical (TB-LMTO and FPLO) EDs. All three ED patterns are in good agreement and support a model that features covalent interaction within the boron layers and non-directed Mg—B interactions. The two theoretical methods give a charge transfer of 1.5 or 1.6 e from the Mg atom to the boron network, in good agreement with the values of 1.4 e obtained from the reconstructed density and 1.5 e resulting from bonding analysis with an electron-localization function (Schmidt *et al.*, 2003).

VT gratefully acknowledges the Max-Planck-Gesellschaft for financial support. This work was partially supported by the New Energy and Industrial Technology Development Organization (NEDO) as Collaborative Research and Development of Fundamental Technologies for Superconductivity Applications. The authors thank F. R. Wagner for valuable discussions.

References

Akselrud, L. G., Grin, Yu., Zavaliy, P. Yu. & Pecharsky, V. K. (1990). *The 2nd Conference on Accurate Structural Studies of Crystals*, Riga, Abstracts, p. 158.

An, J. M. & Pickett, W. E. (2001). *Phys. Rev. Lett.* **86**, 4366–4369.

Andersen, O. K., Pawlowska, Z. & Jepsen, O. (1986). *Phys. Rev. B*, **34**, 5253–5269.

Bader, R. F. W. (1990). In *Atoms in Molecules: A Quantum Theory*. Oxford: Clarendon Press.

Bader, R. F. W. & Beddall, P. M. (1972). *J. Chem. Phys.* **56**, 3320–3329.

Barth, U. & Hedin, L. (1972). *J. Phys. C*, **5**, 1629–1635.

Becker, P. & Coppens, P. (1974). *Acta Cryst.* A**30**, 129–147.

Belashchenko, K. D., van Schilfgaarde, M. & Antropov, V. P. (2001). *Phys. Rev. B*, **64**, 092503.

Burkhardt, U., Gurin, V. N., Haarmann, F., Borrmann, H., Schnelle, W., Yaresko, A. & Grin, Yu. (2003). Accepted for publication.

Eschrig, H. (1989). In *Optimized LCAO Method and the Electronic Structure of Extended Systems*. Berlin: Springer.

Espinosa, E., Molins, E. & Lecomte, C. (1998). *Chem. Phys. Lett.* **285**, 170–173.

Gerashenko, A., Mikhalev, K., Verkhovskii, S., D'yachkova, T., Tyutyunnik, A. & Zubkov, V. (2002). *Cond.-mat.* 0102421.

Goncharov, A. F., Struzhkin, V. V., Gregoryanz, E., Hu, J. Z., Hemley, R. J., Mao, H. K., Lapertot, G., Bud'ko, S. L. & Canfirld, P. C. (2001). *Phys. Rev. B*, **64**, 100509.

Haas, H. (2001). *Hyperfine Interact.* **136/137**, 731–735.

Hansen, N. & Coppens, P. (1978). *Acta Cryst.* A**34**, 909–921.

Jiang, B., He, H., Zuo, J. M., Yu, R. C., Li, S. C., Qin, C. Q. & Spence, J. C. H. (2002). *Acta Cryst.* A**58**, C173.

Jepsen, O. & Andersen, O. K. (1999). *TB-LMTO-ASA*. Version 4.7. Max-Planck-Institut für Festkörperforschung, Stuttgart, Germany.

Keith, T. A., Bader, R. F. W. & Aray, Y. (1996). *Int. J. Quantum Chem.* **57**, 183–198.

Kirzhnits, D. A. (1957). *Sov. Phys. JETP*, **5**, 64–72.

Koepernik, K. & Eschrig, H. (1999). *Phys. Rev. B*, **59**, 1743–1757.

Kohout, M. (2002). *BASIN*. Version 2.4. Max-Planck-Institut für Chemische Physikfester Stoffe, Dresden, Germany.

Kortus, J., Mazin, I. I., Belashchenko, K. D., Antropov, V. P. & Boyer, L. L. (2001). *Phys. Rev. Lett.* **86**, 4656–4659.

Kunc, K., Loa, I., Syassen, K., Kremer, R. K. & Ahn, K. (2001). *J. Phys. Condens. Matter*, **13**, 9945–9962.

Lee, S., Mori, H., Masui, T., Eltsev, Yu., Yamamoto, A. & Tajima, S. (2001). *J. Phys. Soc. Jpn*, **70**, 2255–2258.

Luana, V., Costales, A. & Martin Pendas, A. (1997). *Phys. Rev. B*, **55**, 4285–4297.

Macchi, P. & Coppens, P. (2001). *Acta Cryst.* A**57**, 656–662.

Martin Pendas, A., Costales, A. & Luana, V. (1997). *Phys. Rev. B*, **55**, 4275–4284.

Mazin, I. I. & Antropov, V. P. (2003). *Cond.-mat.* 0212263.

Medvedeva, N. I., Ivanovskii, A. L., Medvedeva, J. E., Freeman, A. J. & Novikov, D. L. (2001). *Phys. Rev. B*, **65**, 052501.

Mori, H., Lee, S., Yamamoto, A., Tajima, S. & Sato, S. (2002). *Phys. Rev. B*, **65**, 092507.

Nagamatsu, J., Nakagawa, N., Muranaka, T., Zenitani, Y. & Akimitsu, J. (2001). *Nature* (*London*), **410**, 63–64.

Nishibori, E., Takata, M., Sakata, M., Tanaka, H., Muranaka, T. & Akimitsu, J. (2001). *J. Phys. Soc. Jpn*, **20**, 2252–2254.

Osorio-Guillen, J. M., Simak, S. I., Wang, Y., Johansson, B. & Ahuja, R. (2002). *Solid State Commun.* **123**, 257–262.

Perdew, J. P. & Wang, Y. (1992). *Phys. Rev. B*, **45**, 13244–13249.

Protas, J. (1997). *MOLDOS*96/*MOLLY PC-DOS*. Personal communication.

Ravindran, P., Vajeeston, P., Vidya, R., Kjekshus, A. & Fjellvag, H. (2001). *Phys. Rev. B*, **64**, 224509.

Rosner, H., Au, J. M., Pickett, W. E. & Drechsler, S.-L. (2002). *Phys. Rev. B*, **66**, 024521.

Sasaki, S., Fujino, K., Takeuchi, Y. & Sadanaga, R. (1980). *Acta Cryst.* A**36**, 904–915.

Schmidt, J., Schnelle, W., Grin, Yu. & Kniep, R. (2003). *Solid State Sci.* **5**, 535–539.

Stash, A. (2002). *MOLDOS*2002/*MOLLY PC-DOS*. Unpublished.

Stash, A. & Tsirelson, V. (2002). *J. Appl. Cryst.* **35**, 371–373.

Tsirelson, V. G. (2002). *Acta Cryst.* B**58**, 632–639.

Tsirelson, V. G. & Ozerov, R. P. (1996). *Electron Density and Bonding in Crystals*. Bristol, England/Philadelphia, USA: Institute of Physics.

Voloshina, I. V., Tsirelson, V. G., Zharikov, E. V., Kalitin, S. P., Gerr, R. G., Antipin, M. Yu., Ozerov, R. P., Struchkov, Yu. T. & Osiko, V. V. (1989). *Dokl. Akad. Nauk SSSR*, **308**, 1115–1118.

Yildirim, T., Guelseren, O., Lynn, J. W., Brown, C. M., Udovic, T. J., Huang, Q., Rogado, N., Regan, K. A., Hayward, M. A., Slusky, J. T., He, T., Haas, M. K., Khalifah, P., Inumaru, K. & Cava, R. J. (2001). *Phys. Rev. Lett.* **87**, 037001.

Zhu, Y., Wu, L., Volkov, V., Li, Q., Gu, G., Moodenbaugh, A. R., Malac, M., Suenaga, M. & Tranquada, J. (2001). *Physica C*, **356**, 239–253.

Zou, P. F. & Bader, R. F. W. (1993). *Acta Cryst.* A**50**, 714–724.